

Radio Maps for Beam Alignment in mmWave Communications with Location Uncertainty

Tien Ngoc Ha, Daniel Romero
Department of ICT, University of Agder
Grimstad, Norway
{tien.n.ha, daniel.romero}@uia.no

Roberto López-Valcarce
atlanTTic Research Center, University of Vigo
Vigo, Spain
valcarce@gts.uvigo.es

Abstract—Next generation communication systems require accurate beam alignment to counteract the impairments that characterize propagation in high-frequency bands. The overhead of the pilot sequences required to select the best beam pair is prohibitive when codebooks contain a large number of beams, as is the case in practice. To remedy this issue, some schemes exploit information about the user location to predict the best beam pair. However, these schemes (i) involve no measurements whatsoever, which generally results in a highly suboptimal predicted beam, and (ii) are not robust to localization errors. To address these limitations, this paper builds upon the notion of radio map to develop two algorithms that attain a balance between the quality of the obtained beam pair and measurement overhead. The proposed algorithms predict the received power corresponding to each pair and measure just the Q pairs with highest prediction. While the first algorithm targets simplicity, the second one relies on a Bayesian approach to endow the prediction process with robustness to localization error. The performance of both algorithms is shown to widely outperform existing methods using ray-tracing data.

Index Terms—Radio maps, beam alignment, mmWave communications, localization.

I. INTRODUCTION

The demand for higher data rates, lower latency, and increased connectivity calls for the development of sixth-generation (6G) communication systems [1]. To support such high data rates, 6G systems are expected to heavily rely on the millimeter-wave (mmWave) frequency band, which spans from 30 GHz to 300 GHz. The propagation impairments that characterize this band, such as high path loss, render beamforming with large antenna arrays necessary at both the transmit and receive sides [2]. To reduce hardware costs, the beamforming vectors are chosen from a finite set, which is referred to as a beam codebook.

The problem of finding the right pair of transmit and receive beamforming vectors in the codebook is known as beam alignment. The simplest approach is the *exhaustive search* method, where the gain of all possible pairs is measured in a *measurement* (or training) *phase* and the pair with greatest measured gain is selected for the *data transmission phase*. Unfortunately, the duration of the measurement phase may

be prohibitive since the number of pairs is typically large in practice. To alleviate this limitation, *hierarchical search* relies on codebooks of beams with nested radiation patterns to find the best pair using the bisection method [3]. However, measurement noise may lead to erroneous decisions in early stages of this search, which can result in the selection of a highly suboptimal pair. This means that a long measurement phase is required to sufficiently average out the noise and thereby obtain accurate gain estimates.

Machine learning-based strategies have been proposed to reduce the measurement overhead of the aforementioned kinds of methods [4]–[6]. For example, [4] predicts the optimal beam based on the measurements of a subset of beams. Inspired by hierarchical search, [6] predicts the optimal narrow beam based on received signal strength (RSS) measurements of wide beams. In [5], the optimal beam is predicted based on the channel matrix measured in a lower-frequency band.

However, these methods do not take into account side information which can be useful to select the optimal pair with lower overhead. To remedy this limitation, [7] predicts the optimal beam based on LiDAR measurements, the location of the base station (BS), and the location of the user equipment (UE). In [2], a radio map that provides the best beam pair index for every UE location is constructed. However, these methods suffer from two limitations: First, (L1) they provide a single beam pair, which is the one to be used for data transmission without previously measuring it. This means that prediction errors may result in a considerable performance degradation. Second, (L2) these methods are not robust to localization errors, which are significant in practice.

The main contributions of this paper aim at overcoming these limitations. The first contribution is an algorithm that predicts the power of each beam pair by constructing a radio map for each of them. Predicting the power rather than the index, as in [2], results in a small collection of candidate beam pairs. Each beam pair is measured and the best one is used for transmission, which effectively solves (L1). The second contribution is an algorithm that extends the first one to take into account localization errors. The pursued Bayesian approach results in a scheme that can cope not only with (L1) but also with (L2). The performance of both algorithms on ray-tracing data is shown to be markedly superior to that of existing methods.

This research has been funded in part by the Research Council of Norway under IKTPLUSS grant 311994 and by MCIN/AEI/10.13039/501100011033/FEDER “A way of making Europe” under project MAYTE (PID2022-136512OB-C22).

The rest of the paper is organized as follows. The system model and problem formulation are presented in Sec. II. Strategies based on radio maps, including the first of the proposed algorithms, are discussed in Sec. III. The second algorithm, which is robust to localization errors, is proposed in Sec. IV. Finally, Secs. V and VI respectively provide simulation results and conclusions.

II. MODEL AND PROBLEM FORMULATION

Let $\mathcal{R} \in \mathbb{R}^d$ comprise the coordinates of all points in the spatial region of interest, where d is typically 2 or 3. Consider a mmWave system that comprises a BS with N_{BS} antennas a UE with N_{UE} antennas. The UE is located at $\mathbf{r} \in \mathcal{R}$. Without loss of generality, the exposition focuses on the downlink, but the proposed methods carry over unaltered to the uplink. The channel matrix will be denoted by $\mathbf{H} \in \mathbb{C}^{N_{\text{UE}} \times N_{\text{BS}}}$.

The beamforming vectors at the BS and UE are respectively denoted by $\mathbf{v} \in \mathbb{C}^{N_{\text{BS}} \times 1}$, and $\mathbf{w} \in \mathbb{C}^{N_{\text{UE}} \times 1}$. Without loss of generality, it is assumed that both vectors are normalized, i.e., $\|\mathbf{v}\|^2 = \|\mathbf{w}\|^2 = 1$. Vectors \mathbf{v} and \mathbf{w} are respectively picked from the codebooks $\mathcal{V} = \{\mathbf{v}_1, \dots, \mathbf{v}_{M_{\text{BS}}}\}$, and $\mathcal{W} = \{\mathbf{w}_1, \dots, \mathbf{w}_{M_{\text{UE}}}\}$, where M_{BS} and M_{UE} are respectively the numbers of transmit and receive beamforming vectors. Usually $M_{\text{BS}} \leq N_{\text{BS}}$ and $M_{\text{UE}} \leq N_{\text{UE}}$. The proposed schemes are applicable to analog, digital, or hybrid beamforming so long as the size of both codebooks is finite. A typical example of a codebook is the *discrete Fourier transform* (DFT) codebook, which for uniform linear arrays (ULAs) contains $\mathbf{v}_{m_{\text{BS}}} = \frac{1}{\sqrt{N_{\text{BS}}}} [1, e^{j\frac{2\pi}{N_{\text{BS}}} m_{\text{BS}}}, \dots, e^{j\frac{2\pi}{N_{\text{BS}}} m_{\text{BS}}(N_{\text{BS}}-1)}]^\top$, $m_{\text{BS}} = 1, \dots, N_{\text{BS}}$, and $\mathbf{w}_{m_{\text{UE}}} = \frac{1}{\sqrt{N_{\text{UE}}}} [1, e^{j\frac{2\pi}{N_{\text{UE}}} m_{\text{UE}}}, \dots, e^{j\frac{2\pi}{N_{\text{UE}}} m_{\text{UE}}(N_{\text{UE}}-1)}]^\top$, $m_{\text{UE}} = 1, \dots, N_{\text{UE}}$.

The signal transmitted by the BS is denoted as $\sqrt{P}s \in \mathbb{C}^1$, where P is the transmit power and $\mathbb{E}[|s|^2] = 1$. Then, the received signal at the UE is given by

$$y(\mathbf{v}, \mathbf{w}) = \sqrt{P}\mathbf{w}^H \mathbf{H} \mathbf{v} s + \mathbf{w}^H \mathbf{n}, \quad (1)$$

where $\mathbf{n} \in \mathbb{C}^{N_{\text{UE}} \times 1}$ is the additive noise at the receiver. Thus, one can define the RSS at the UE as $\gamma(\mathbf{v}, \mathbf{w}) := |\sqrt{P}\mathbf{w}^H \mathbf{H} \mathbf{v}|^2$.

Given \mathcal{V} and \mathcal{W} , the beam alignment problem is to find the beam pair that maximizes the RSS:

$$\max_{\mathbf{v} \in \mathcal{V}, \mathbf{w} \in \mathcal{W}} \gamma(\mathbf{v}, \mathbf{w}). \quad (2)$$

As discussed in Sec. I, existing approaches use different kinds of information to find the optimal pair. The present paper considers the problem of *location-aware beam alignment*, in which a location estimate $\hat{\mathbf{r}}$ of the actual UE location $\mathbf{r} \in \mathcal{R}$ is given. In addition, a set \mathcal{D} of measurements of all beam pairs at J locations is given, specifically $\mathcal{D} := \{(\hat{\mathbf{r}}_j, \tilde{\gamma}_{j, m_{\text{BS}}, m_{\text{UE}}})\}_{j, m_{\text{BS}}, m_{\text{UE}}}$, where $\tilde{\gamma}_{j, m_{\text{BS}}, m_{\text{UE}}}$ is the measured RSS for the beam pair $(\mathbf{v}_{m_{\text{BS}}}, \mathbf{w}_{m_{\text{UE}}})$ at the j -th location $\mathbf{r}_j \in \mathcal{R}$ and $\hat{\mathbf{r}}_j$ is an estimate of \mathbf{r}_j , which in practice is obtained using localization techniques such as GPS.

The problem of location-aware beam alignment is addressed first in Sec. III for the case where there is no location

uncertainty, that is, $\hat{\mathbf{r}} = \mathbf{r}$ and $\hat{\mathbf{r}}_j = \mathbf{r}_j$ for all j . The case where there is location uncertainty is addressed in Sec. IV.

III. RADIO MAP-BASED BEAM ALIGNMENT

This section discusses approaches to solve the beam alignment problem using radio maps. To bypass the limitations of existing schemes, a new algorithm is proposed at the end of the section.

The simplest form of location-aware beam alignment algorithm arises when propagation takes place in free space and the location and orientation of the BS and UE are known. In this case, one can compute the angle of arrival (AoA) and the angle of departure (AoD) and choose the best beam pair based on the radiation pattern of each beam [8]. However, in practice, there are obstacles that can block the line of sight path, which renders this method ineffective.

To address this limitation, radio maps can be used. Radio maps provide a radio frequency (RF) metric at each spatial location of a geographical area [9]–[18]. Possible RF metrics include the RSS, channel gain, power spectral density, and so on. Radio maps are commonly estimated by interpolating measurements acquired across the area of interest.

One approach for location-aware beam alignment using radio maps can be found in [2]. The scheme proposed therein constructs radio maps of the AoA, AoD, and gain of each path from the BS to every possible UE location. Using the Saleh-Valenzuela model [19], \mathbf{H} is reconstructed at \mathbf{r} based on these quantities and then used to estimate the RSS for each beam pair. Unfortunately, spatially interpolating the aforementioned path parameters (AoAs, AoDs, and gains) to evaluate the radio maps is challenging because one cannot readily determine the correspondence between paths at different locations.

To sidestep this challenge, [2] also proposes constructing a “beam index map” (BIM) that provides the index of the best beam pair for every UE location. This beam is directly utilized in the transmission phase without any measurement phase. Unfortunately, although this eliminates the measurement overhead, the beam provided by the map may be highly suboptimal, especially in areas where \mathcal{D} contains few measurement locations. Also, this approach applies K-nearest neighbor (KNN) interpolation to the beam indices, which seems problematic in practice as beam indices are discrete and, therefore, their averages may not capture the relations between the radiation patterns of the beams in the codebook.

To address these limitations, the first algorithm proposed here constructs a radio map for each beam pair. Specifically, for each $(m_{\text{BS}}, m_{\text{UE}})$, the data $\{(\mathbf{r}_j, \tilde{\gamma}_{j, m_{\text{BS}}, m_{\text{UE}}})\}_j$ is used to construct a radio map that provides an estimate of the RSS $\gamma_{m_{\text{BS}}, m_{\text{UE}}}$ at each possible UE location \mathbf{r} . Fig. 1 shows two examples of radio maps for two different beam pairs. As can be seen, the RSS is location-dependent and varies differently across space for different beam pairs.

These $M_{\text{BS}}M_{\text{UE}}$ radio maps can be constructed using any technique for power map estimation [9]. However, since $M_{\text{BS}}M_{\text{UE}}$ may be large, it is desirable to keep complexity low. To this end, KNN with 1 neighbor may be suitable since it

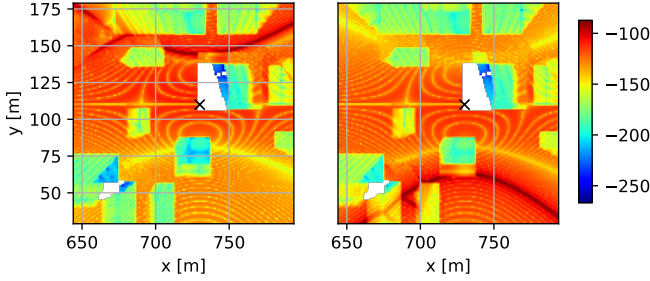


Fig. 1: Examples of radio maps for two beam pairs. The black crosses represent the BS location.

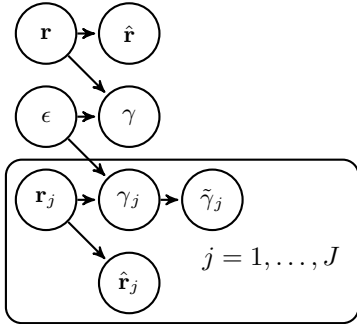


Fig. 2: Graphical model of the system.

just requires storing \mathcal{D} and finding $\arg \min_j \|\mathbf{r} - \mathbf{r}_j\|$ for each new \mathbf{r} . This computation need not be performed for each beam pair but once for all pairs. After predicting the power of each beam pair at \mathbf{r} using the radio maps, the Q beam pairs with the highest power estimates are measured in the measurement phase. Based on the resulting measurements, the best of these pairs is selected for the data transmission phase.

This algorithm will be referred to as *radio MAP BEam aLignment* (MABEL).

IV. RADIO MAP-BASED BEAM ALIGNMENT WITH LOCATION UNCERTAINTY

The approaches in Sec. III assume that the UE location is perfectly known, but this is not the case in practice. Location error can be caused e.g. by multipath, the inaccuracy of the localization system, and the mobility of the UE. This section builds upon Bayesian principles to develop an improved version of MABEL where the interpolation technique used to construct the radio maps is robust to location errors.

To this end, a probabilistic model must be adopted. Such a model is represented by the Bayesian network in Fig. 2. Recall that Bayesian networks constitute a special kind of graphical model [20, Ch. 8]. This network captures the conditional independence relations among the considered random variables. The subscripts corresponding to the beam indices have been omitted to simplify notation. The procedure described in this section needs to be applied for each beam pair. Circles denote random variables, and arrows denote the conditional

dependencies. The model is fully defined by specifying the probability density functions (PDFs) of each random variable conditioned on its parents on the graph, namely $p(\mathbf{r})$, $p(\hat{\mathbf{r}}|\mathbf{r})$, $p(\epsilon)$, $p(\gamma|\mathbf{r}, \epsilon)$, $p(\mathbf{r}_j)$, $p(\gamma_j|\mathbf{r}, \epsilon)$, $p(\hat{\mathbf{r}}_j|\mathbf{r}_j)$ and $p(\tilde{\gamma}_j|\gamma_j)$. The product of these PDFs is the joint PDF of all the random variables in the model. A non-informative prior is adopted for $p(\mathbf{r})$ whereas $p(\hat{\mathbf{r}}|\mathbf{r})$ is multivariate Gaussian $\mathcal{N}(\hat{\mathbf{r}}|\mathbf{r}, \mathbf{C})$. The same applies to $p(\mathbf{r}_j)$ and $p(\hat{\mathbf{r}}_j|\mathbf{r}_j)$. Variable ϵ captures the propagation environment as well as all parameters and locations of the transmitters. This variable is used to express the RSS as a deterministic function of the location and the environment: $\gamma = g(\epsilon, \mathbf{r})$ and $\gamma_j = g(\epsilon, \mathbf{r}_j)$, which in turn determine $p(\gamma|\mathbf{r}, \epsilon)$ and $p(\gamma_j|\mathbf{r}_j, \epsilon)$. In a simulation, ϵ could play the role of the 3D model of the environment and g could be the ray-tracing software. The variable ϵ is not explicitly modeled, which means that $p(\epsilon)$ and g will be unknown. Finally, $p(\tilde{\gamma}_j|\gamma_j)$ can be assumed to be e.g. $\mathcal{N}(\tilde{\gamma}_j|\gamma_j, \sigma_z^2)$, where σ_z^2 is the variance of the additive measurement noise.

Ideally, one would like to obtain the minimum mean square error (MMSE) estimator for the RSS. Applying a well-known result in estimation theory [21], the MMSE estimator is given by $\mathbb{E}[\gamma|\hat{\mathbf{r}}, \mathcal{D}]$. To obtain this conditional expectation, observe that

$$p(\gamma|\hat{\mathbf{r}}, \mathcal{D}) = \int_{\mathbf{r} \in \mathcal{R}} p(\gamma, \mathbf{r}|\hat{\mathbf{r}}, \mathcal{D}) d\mathbf{r} \quad (3a)$$

$$= \int_{\mathbf{r} \in \mathcal{R}} p(\gamma|\mathbf{r}, \hat{\mathbf{r}}, \mathcal{D}) p(\mathbf{r}|\hat{\mathbf{r}}, \mathcal{D}) d\mathbf{r} \quad (3b)$$

$$= \int_{\mathbf{r} \in \mathcal{R}} p(\gamma|\mathbf{r}, \mathcal{D}) p(\mathbf{r}|\hat{\mathbf{r}}) d\mathbf{r} \quad (3c)$$

$$\approx \frac{\sum_{j=1}^J p(\mathbf{r} = \hat{\mathbf{r}}_j|\hat{\mathbf{r}}) p(\gamma|\mathbf{r} = \hat{\mathbf{r}}_j, \mathcal{D})}{\sum_{j=1}^J p(\mathbf{r} = \hat{\mathbf{r}}_j|\hat{\mathbf{r}})}. \quad (3d)$$

Here, (3c) follows from the fact that γ is conditionally independent of $\hat{\mathbf{r}}$ given \mathbf{r} and $p(\mathbf{r}|\hat{\mathbf{r}}) = p(\mathbf{r}|\hat{\mathbf{r}}, \mathcal{D})$, which follows from the D-separation rules [20, Sec. 8.2.2], and (3d) is just a discrete approximation of the integral.

From (3), it follows that

$$\mathbb{E}[\gamma|\hat{\mathbf{r}}, \mathcal{D}] \approx \frac{\sum_{j=1}^J p(\mathbf{r} = \hat{\mathbf{r}}_j|\hat{\mathbf{r}}) \mathbb{E}[\gamma|\mathbf{r} = \hat{\mathbf{r}}_j, \mathcal{D}]}{\sum_{j=1}^J p(\mathbf{r} = \hat{\mathbf{r}}_j|\hat{\mathbf{r}})} \quad (4a)$$

$$= \frac{\sum_{j=1}^J \exp(-\frac{1}{2}(\hat{\mathbf{r}}_j - \hat{\mathbf{r}})^\top \mathbf{C}^{-1}(\hat{\mathbf{r}}_j - \hat{\mathbf{r}})) \mathbb{E}[\gamma|\mathbf{r} = \hat{\mathbf{r}}_j, \mathcal{D}]}{\sum_{j=1}^J \exp(-\frac{1}{2}(\hat{\mathbf{r}}_j - \hat{\mathbf{r}})^\top \mathbf{C}^{-1}(\hat{\mathbf{r}}_j - \hat{\mathbf{r}}))}, \quad (4b)$$

where it was used that

$$p(\mathbf{r} = \hat{\mathbf{r}}_j|\hat{\mathbf{r}}) = \frac{p(\mathbf{r} = \hat{\mathbf{r}}_j, \hat{\mathbf{r}})}{p(\hat{\mathbf{r}})} = \frac{p(\hat{\mathbf{r}}|\mathbf{r} = \hat{\mathbf{r}}_j) p(\mathbf{r} = \hat{\mathbf{r}}_j)}{p(\hat{\mathbf{r}})} \quad (5a)$$

$$= p(\hat{\mathbf{r}}|\mathbf{r} = \hat{\mathbf{r}}_j) \quad (5b)$$

by assuming uniform priors for \mathbf{r} and $\hat{\mathbf{r}}$. Observe that (5), when seen as a function of $\hat{\mathbf{r}}$, is a radio map that provides the RSS of a beam pair.

The rest of this section approximates $\mathbb{E}[\gamma|\mathbf{r} = \hat{\mathbf{r}}_j, \mathcal{D}]$ in the cases without and with localization error in the locations in

D. Suppose first that there is no localization error in these locations, i.e., $\mathbf{r}_j = \hat{\mathbf{r}}_j, j = 1, \dots, J$. As a result

$$\mathbb{E}[\gamma|\mathbf{r} = \hat{\mathbf{r}}_j, \mathcal{D}] = \mathbb{E}[\gamma|\mathbf{r} = \mathbf{r}_j, \mathcal{D}] \quad (6a)$$

$$\stackrel{A}{=} \mathbb{E}[\gamma_j|\mathbf{r} = \mathbf{r}_j, \mathcal{D}] \stackrel{B}{=} \mathbb{E}[\gamma_j|\mathcal{D}] \quad (6b)$$

$$= \mathbb{E}[\gamma_j|\mathbf{r}_j, \tilde{\gamma}_j, \mathcal{D}_j] \approx \mathbb{E}[\gamma_j|\tilde{\gamma}_j], \quad (6c)$$

where (A) follows from the fact that if $\mathbf{r} = \mathbf{r}_j$, then $\gamma = g(\epsilon, \mathbf{r}) = g(\epsilon, \mathbf{r}_j) = \gamma_j$, (B) follows from the D-separation rules, $\mathcal{D}_j := \mathcal{D} \setminus \{\hat{\mathbf{r}}_j, \tilde{\gamma}_j\}$, and the approximation in (6c) is explained in Appendix A. If, for example, γ has PDF $\mathcal{N}(\gamma|\mu_\gamma, \sigma_\gamma^2)$ and is independent of z , then, it is easy to show that

$$\mathbb{E}[\gamma_j|\tilde{\gamma}_j] = \mu_\gamma + \frac{\sigma_\gamma^2}{\sigma_\gamma^2 + \sigma_z^2}(\tilde{\gamma}_j - \mu_\gamma). \quad (7)$$

On the other hand, in the presence of localization error, one needs to introduce further approximations. Start by noting that

$$\mathbb{E}[\gamma|\mathbf{r} = \hat{\mathbf{r}}_j, \mathcal{D}] \quad (8a)$$

$$= \int \mathbb{E}[\gamma|\hat{\mathbf{r}}, \mathbf{r} = \hat{\mathbf{r}}_j, \mathcal{D}] p(\hat{\mathbf{r}}|\mathbf{r} = \hat{\mathbf{r}}_j, \mathcal{D}) d\hat{\mathbf{r}} \quad (8b)$$

$$\approx \frac{\sum_{j'=1}^J p(\hat{\mathbf{r}} = \hat{\mathbf{r}}_{j'}|\mathbf{r} = \hat{\mathbf{r}}_j) \mathbb{E}[\gamma|\hat{\mathbf{r}} = \hat{\mathbf{r}}_{j'}, \mathbf{r} = \hat{\mathbf{r}}_j, \mathcal{D}]}{\sum_{j'=1}^J p(\hat{\mathbf{r}} = \hat{\mathbf{r}}_{j'}|\mathbf{r} = \hat{\mathbf{r}}_j)}, \quad (8c)$$

where $p(\hat{\mathbf{r}}|\mathbf{r} = \hat{\mathbf{r}}_j, \mathcal{D}) = p(\hat{\mathbf{r}}|\mathbf{r} = \hat{\mathbf{r}}_j)$ follows from the D-separation rules.

To obtain $\mathbb{E}[\gamma|\hat{\mathbf{r}} = \hat{\mathbf{r}}_{j'}, \mathbf{r} = \hat{\mathbf{r}}_j, \mathcal{D}]$, suppose that, if $\hat{\mathbf{r}} = \hat{\mathbf{r}}_i$, then $\mathbf{r} = \mathbf{r}_i$. This assumption is justified if (i) $\hat{\mathbf{r}}$ (resp. $\hat{\mathbf{r}}_i$) is a deterministic function of \mathbf{r} (resp. \mathbf{r}_i) and the environment ϵ , and (ii) this function is injective for each ϵ . In practice, these two conditions may not exactly hold but they constitute a reasonable approximation. It follows that, if $\hat{\mathbf{r}} = \hat{\mathbf{r}}_i$, then $\gamma = g(\epsilon, \mathbf{r}) = g(\epsilon, \mathbf{r}_i) = \gamma_i$. Therefore,

$$\mathbb{E}[\gamma|\hat{\mathbf{r}} = \hat{\mathbf{r}}_{j'}, \mathbf{r} = \hat{\mathbf{r}}_j, \mathcal{D}] \quad (9a)$$

$$= \mathbb{E}[\gamma_{j'}|\hat{\mathbf{r}} = \hat{\mathbf{r}}_{j'}, \mathbf{r} = \hat{\mathbf{r}}_j, \mathbf{r}_{j'} = \hat{\mathbf{r}}_j, \mathcal{D}] \quad (9b)$$

$$= \mathbb{E}[\gamma_{j'}|\mathbf{r}_{j'} = \hat{\mathbf{r}}_j, \mathcal{D}] \quad (9c)$$

$$= \mathbb{E}[\gamma_{j'}|\mathbf{r}_{j'} = \hat{\mathbf{r}}_j, \hat{\mathbf{r}}_{j'}, \tilde{\gamma}_{j'}, \mathcal{D}_{j'}] \quad (9d)$$

$$= \mathbb{E}[\gamma_{j'}|\mathbf{r}_{j'} = \hat{\mathbf{r}}_j, \tilde{\gamma}_{j'}, \mathcal{D}_{j'}] \quad (9e)$$

$$\approx \mathbb{E}[\gamma_{j'}|\tilde{\gamma}_{j'}], \quad (9f)$$

where (9c) and (9e) follow from the D-separation rules and (9f) follows from the same arguments as in Appendix A. Finally, $\mathbb{E}[\gamma_{j'}|\tilde{\gamma}_{j'}]$ can be obtained e.g. as in (7).

Once the RSS of all beam pairs has been estimated, the algorithm proceeds as MABEL: the Q beam pairs with the highest power estimates are measured in the measurement phase. The improved version of MABEL proposed in this section will be referred to as *LOcation-Robust bEam alignment* (LOREN).

V. SIMULATION RESULTS

In this section, the performance of the proposed beam alignment strategies is evaluated through synthetic data from ray-tracing software and compared with existing beam alignment methods.

To this end, a channel matrix is generated using ray-tracing for each UE location in a grid with 1 m spacing constructed in a square urban scenario with a side of 150 m. The carrier frequency is 30 GHz, the bandwidth is 1 MHz, $N_{\text{BS}} = 16$, and $N_{\text{UE}} = 4$. The transmit power is $P = 0$ dBm, so that the values of RSS reported here can also be interpreted as gain. DFT codebooks are used in all cases. To focus on spatial interpolation effects and the impact of the location error, no measurement noise is introduced. The location estimates are generated as $\hat{\mathbf{r}} \sim \mathcal{N}(\mathbf{r}, \sigma_{\text{test}}^2 \mathbf{I}_2)$ and $\hat{\mathbf{r}}_j \sim \mathcal{N}(\mathbf{r}_j, \sigma_{\text{train}}^2 \mathbf{I}_2)$.

The following benchmarks are considered: (i) Exhaustive search beam alignment (ESBA): the best beam pair is chosen by measuring all possible beam pairs. Location information and \mathcal{D} are not used. (ii) Hierarchical search beam alignment (HSBA) with $\log_2(N_{\text{BS}})$ levels at the BS and $\log_2(N_{\text{UE}})$ levels at the UE. Each level involves measuring the four possible beam pairs in that level. Location information and \mathcal{D} are not used. (iii) The BIM algorithm from [2] with 5 neighbors. To improve its performance, instead of averaging beam indices, the optimal beams at the 5 nearest neighbors are measured.

At every Monte Carlo iteration, J locations are randomly selected from the grid to form \mathcal{D} . A set of test locations \mathbf{r} is randomly selected from the remaining grid points to average the performance metrics. For each of those testing locations, each algorithm returns a sorted list with the order in which the beams must be measured. ESBA and BIM must measure all the beam pairs in the list, MABEL and LOREN just measure the first Q pairs in the list to choose the best, and HSBA adaptively creates this list based on previous measurements.

To analyze performance for all possible values of Q at the same time, the adopted metrics should therefore assess the ability of an algorithm to return strong beam pairs at the beginning of the list. In particular, the following metrics are considered: (i) *The best measured beam power so far* (BMBPSF) is the sequence of maxima of the true (not measured) RSS of each beam in the order of the list returned by the tested algorithm. The faster it grows at the beginning, the better. (ii) The number of measured beam pairs (NMBP) to reach an RSS that is within a given margin from the best beam pair.

In all experiments, LOREN assumes $p(\hat{\mathbf{r}}|\mathbf{r}) = \mathcal{N}(\hat{\mathbf{r}}|\mathbf{r}, \hat{\sigma}_{\text{test}}^2 \mathbf{I}_2)$ and $p(\hat{\mathbf{r}}_j|\mathbf{r}_j) = \mathcal{N}(\hat{\mathbf{r}}_j|\mathbf{r}_j, \hat{\sigma}_{\text{train}}^2 \mathbf{I}_2)$, where $\hat{\sigma}_{\text{train}}^2$ and $\hat{\sigma}_{\text{test}}^2$ need not equal the parameters σ_{train}^2 and σ_{test}^2 used to generate the data.

The first step is to investigate the robustness of the considered algorithms with respect to the error in $\hat{\mathbf{r}}$. To this end, σ_{train} will be initially set to 0. Fig. 3 shows the BMBPSF sequence for the considered algorithms when $\sigma_{\text{test}} = 25$ m. The left-most point in each curve provides the true RSS of the first measured pair. This RSS is greater for the algorithms based on radio maps (BIM, MABEL, LOREN) than for the location-agnostic algorithms (ESBA, HSBA), which shows the benefits of exploiting location information. The RSS of the first measured beam pair is the same for BIM and MABEL. This is because the interpolation algorithm adopted by MABEL was KNN with 1 neighbor and, therefore, the first measured pair

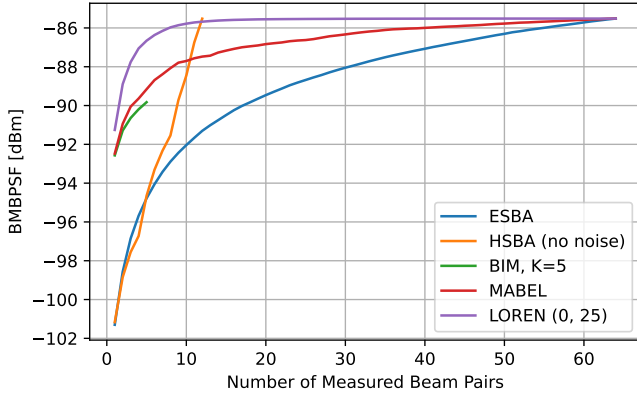


Fig. 3: BMBPSF vs. the number of measurements when $\sigma_{\text{test}} = 25$ m and $J = 500$. The legend entries of LOREN indicate $(\hat{\sigma}_{\text{train}}, \hat{\sigma}_{\text{test}})$.

in both cases is the best beam pair at the nearest neighbor in \mathcal{D} . Except for BIM, which measures only 5 beams, the rest of algorithms eventually reach the maximum RSS. ESBA is the slowest algorithm. This is expected as this is the one that uses the smallest amount of information. HSBA reaches the maximum RSS faster than ESBA, which is reasonable since it creates the list of beam pairs to measure adaptively based on previous measurements. The BMBPSF of MABEL grows faster than BIM, which shows the benefits of interpolating RSS rather than just mapping beam pair indices. The BMBPSF of LOREN is the one that grows fastest because of its robustness to the localization error in $\hat{\mathbf{r}}$. Observe that it roughly reaches the maximum power with just 10 measurements. This means that Q can be set to 10. Although this number is similar to the number of measurements required by HSBA to reach the maximum in Fig. 3, the fact that no measurement noise is considered means that the curve for HSBA is just an upper bound. In practice, the curve for HSBA will be lower, meaning that it does not reach the maximum. In other words, when there is measurement noise, the mean power of the beam obtained by HSBA is lower than the mean power of the best beam.

Observe that LOREN requires knowledge of σ_{train} and σ_{test} . In practice, these parameters may not be accurately known. Thus, it is important to assess the impact of a mismatch between the true and the assumed values of σ_{train} and σ_{test} on the performance of this algorithm. To this end, Fig. 4 plots NMBP with margin 1 dB versus σ_{test} for several values of $\hat{\sigma}_{\text{test}}$. As expected, the NMBP of the proposed algorithms increases with σ_{test} . The NMBP of ESBA and HSBA is not affected by σ_{test} because they do not utilize $\hat{\mathbf{r}}$. Similarly to the previous experiment, the curve for HSBA is overly optimistic about the actual performance of this algorithm: in the presence of measurement noise, HSBA may not always find the best beam pair, which means that NMBP is undefined. Observe that, for each σ_{test} , the smallest NMBP is obtained by LOREN when $\hat{\sigma}_{\text{test}} = \sigma_{\text{test}}$. Note also that the performance degradation is more significant if $\hat{\sigma}_{\text{test}} < \sigma_{\text{test}}$ than if $\hat{\sigma}_{\text{test}} > \sigma_{\text{test}}$, which

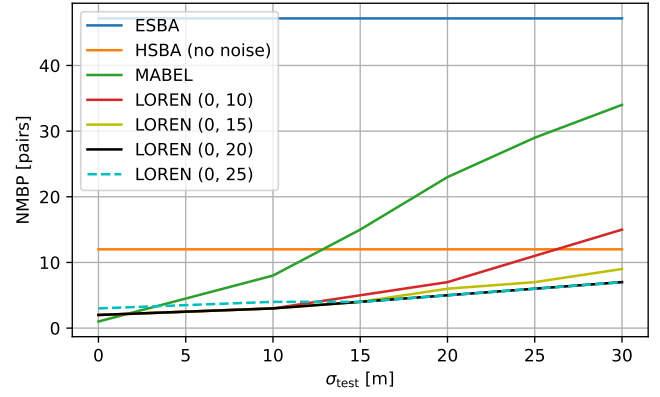


Fig. 4: NMBP with margin = 1 dB vs. σ_{test} . The legend entries of LOREN indicate $(\hat{\sigma}_{\text{train}}, \hat{\sigma}_{\text{test}})$.

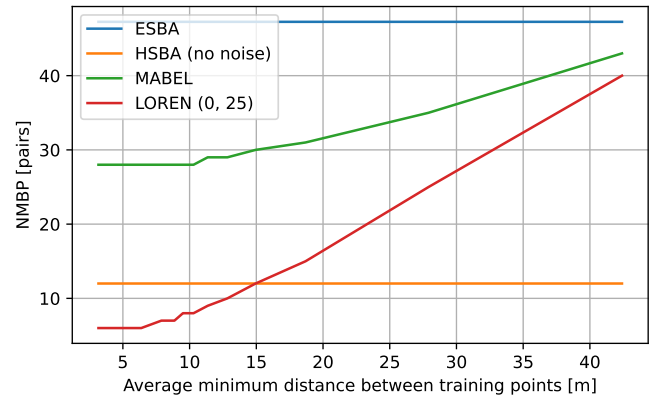


Fig. 5: NMBP with a given margin = 1 dB vs. the average minimum distance between locations in \mathcal{D} when $\sigma_{\text{test}} = 25$ m. The legend entries of LOREN indicate $(\hat{\sigma}_{\text{train}}, \hat{\sigma}_{\text{test}})$.

motivates overestimating σ_{test} . For the specific setup in this experiment, it seems that $\hat{\sigma}_{\text{test}} = 20$ m yields almost the best performance for all considered values of σ_{test} .

Clearly, the performance of the algorithms using \mathcal{D} is determined by J or, equivalently, by the spatial density of the measurement locations in \mathcal{D} , which determines the cost of deploying these algorithms in practice. To investigate this effect, Fig. 5 depicts the NMBP with margin = 1 dB versus the average distance between one location in \mathcal{D} and the nearest location in \mathcal{D} . Each point in the curves is obtained by setting a different J . As before, NMBP for ESBA and HSBA remains constant because these algorithms do not use \mathcal{D} . In the case of HSBA, this is again an overly optimistic curve shown here just as a reference. As any algorithm based on radio maps, the performance of the proposed schemes improves with the spatial density of the locations in \mathcal{D} . Observe that with a spacing of 10 m between locations in \mathcal{D} , LOREN and MABEL approximately achieve their optimal performance.

To analyze how the considered algorithms scale to systems with a large number of antennas, Fig. 6 shows the NBPM with

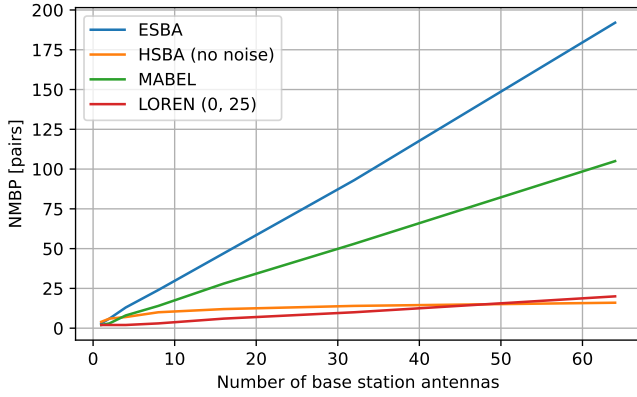


Fig. 6: NMBP with a given margin = 1 dB vs. number of base station antennas when $\sigma_{\text{test}} = 25$ m. The legend entries of LOREN indicate $(\hat{\sigma}_{\text{train}}, \hat{\sigma}_{\text{test}})$.

margin = 1 dB vs. N_{BS} . As expected, the NBPM increases with the number of base station antennas since the number of beam pairs increases. LOREN results in the lowest number of measurements to find a sufficiently good beam. Again, the curve for HSBA is just shown as a reference since it is obtained without measurement noise.

The last experiment quantifies the effect of error in the locations in \mathcal{D} . To this end, the BMBPSF sequence is shown for different σ_{train} and σ_{test} in Figs. 7 and 8. It is observed that the performance of MABEL is drastically deteriorated with both σ_{train} and σ_{test} . In contrast, LOREN is only slightly affected by the location error. Besides, LOREN is not highly sensitive to the choice of $\hat{\sigma}_{\text{train}}$ and $\hat{\sigma}_{\text{test}}$. For this algorithm, it is generally desirable to know the actual σ_{train} and σ_{test} . Against intuition, Fig. 8 shows that a mismatch in these parameters can sometimes lead to an insignificant performance improvement. The reason is that LOREN is not a true MMSE estimator but rather an approximation.

VI. CONCLUSIONS

The problem of location-aware beam alignment was considered. To sidestep the limitations of existing algorithms when measurement locations are exactly known, this paper proposed MABEL, which relies on radio maps that predict the RSS of each beam pair at the UE location. To accommodate location errors, LOREN extends MABEL by capitalizing on a Bayesian approach. Extensive simulations with ray-tracing data showcase the merits of these algorithms relative to the existing alternatives.

APPENDIX A APPROXIMATION IN (6c)

To approximate $\mathbb{E}[\gamma_j | \mathbf{r}_j, \tilde{\gamma}_j, \mathcal{D}_j] \approx \mathbb{E}[\gamma_j | \tilde{\gamma}_j]$, start by noting that $p(\gamma_j, \mathbf{r}_j, \tilde{\gamma}_j, \mathcal{D}_j) = p(\gamma_j | \mathbf{r}_j, \tilde{\gamma}_j, \mathcal{D}_j)p(\mathbf{r}_j, \tilde{\gamma}_j, \mathcal{D}_j)$. Since the g is unknown, it will be assumed that $p(\gamma_j | \mathbf{r}_j, \tilde{\gamma}_j, \mathcal{D}_j) \approx p(\gamma_j | \mathbf{r}_j, \tilde{\gamma}_j)$, which essentially means that the measurement $\tilde{\gamma}_j$ at a certain location \mathbf{r}_j is much more

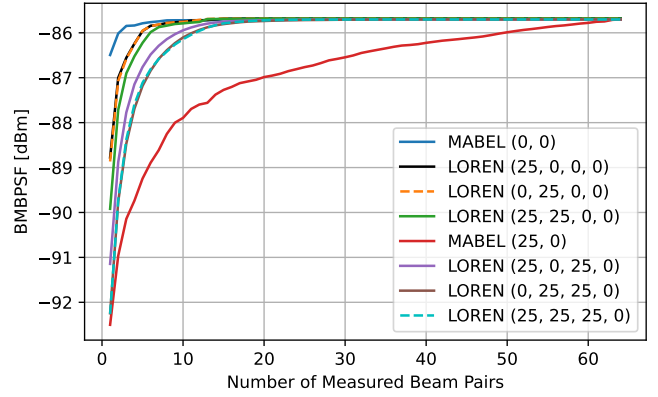


Fig. 7: BMBPSF vs. the number of measured beam pairs for MABEL $(\sigma_{\text{train}}, \sigma_{\text{test}})$ and LOREN $(\hat{\sigma}_{\text{train}}, \hat{\sigma}_{\text{test}}, \sigma_{\text{train}}, \sigma_{\text{test}})$ when $J = 500$.

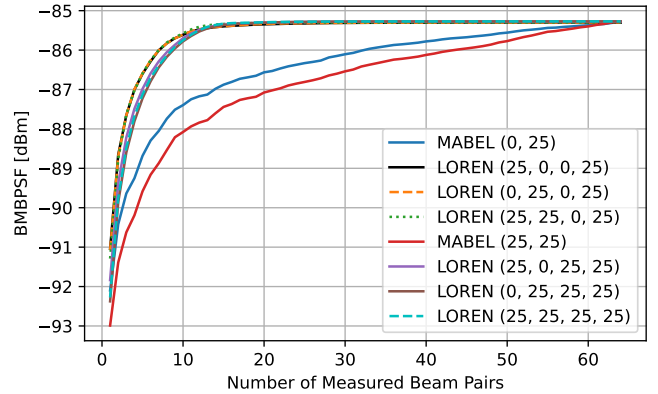


Fig. 8: BMBPSF vs. the number of measured beam pairs for MABEL $(\sigma_{\text{train}}, \sigma_{\text{test}})$ and LOREN $(\hat{\sigma}_{\text{train}}, \hat{\sigma}_{\text{test}}, \sigma_{\text{train}}, \sigma_{\text{test}})$ when $J = 500$.

informative about γ_j than the measurements at the remaining locations. The right-hand side of this expression can also be written as

$$p(\gamma_j | \mathbf{r}_j, \tilde{\gamma}_j) \propto \int p(\gamma_j, \epsilon, \mathbf{r}_j, \tilde{\gamma}_j) d\epsilon \quad (10a)$$

$$= \int p(\tilde{\gamma}_j | \gamma_j, \epsilon, \mathbf{r}_j) p(\gamma_j | \epsilon, \mathbf{r}_j) p(\epsilon) p(\mathbf{r}_j) d\epsilon \quad (10b)$$

$$= \int p(\tilde{\gamma}_j | \gamma_j) p(\gamma_j | \epsilon, \mathbf{r}_j) p(\epsilon) p(\mathbf{r}_j) d\epsilon \quad (10c)$$

$$= p(\tilde{\gamma}_j | \gamma_j) p(\mathbf{r}_j) \int p(\gamma_j | \epsilon, \mathbf{r}_j) p(\epsilon) d\epsilon \quad (10d)$$

$$= p(\mathbf{r}_j) p(\tilde{\gamma}_j | \gamma_j) p(\gamma_j | \mathbf{r}_j), \quad (10e)$$

where (10c) follows from the D-separation rules. Therefore,

$$p(\gamma_j, \mathbf{r}_j, \tilde{\gamma}_j, \mathcal{D}_j) \approx \frac{p(\mathbf{r}_j, \tilde{\gamma}_j, \mathcal{D}_j) p(\mathbf{r}_j) p(\tilde{\gamma}_j | \gamma_j) p(\gamma_j | \mathbf{r}_j)}{\int p(\mathbf{r}_j) p(\tilde{\gamma}_j | \gamma_j) p(\gamma_j | \mathbf{r}_j) d\gamma_j} \quad (11a)$$

$$= \frac{p(\mathbf{r}_j, \tilde{\gamma}_j, \mathcal{D}_j) p(\tilde{\gamma}_j | \gamma_j) p(\gamma_j | \mathbf{r}_j)}{\int p(\tilde{\gamma}_j | \gamma_j) p(\gamma_j | \mathbf{r}_j) d\gamma_j}. \quad (11b)$$

As a result,

$$p(\gamma_j | \mathbf{r}_j, \tilde{\gamma}_j, \mathcal{D}_j) = \frac{p(\gamma_j, \mathbf{r}_j, \tilde{\gamma}_j, \mathcal{D}_j)}{\int p(\gamma_j, \mathbf{r}_j, \tilde{\gamma}_j, \mathcal{D}_j) d\gamma_j} \quad (12a)$$

$$\approx \frac{p(\tilde{\gamma}_j | \gamma_j) p(\gamma_j | \mathbf{r}_j)}{\int p(\tilde{\gamma}_j | \gamma_j) p(\gamma_j | \mathbf{r}_j) d\gamma_j} \stackrel{A}{=} \frac{p(\tilde{\gamma}_j | \gamma_j) p(\gamma_j)}{\int p(\tilde{\gamma}_j | \gamma_j) p(\gamma_j) d\gamma_j} \quad (12b)$$

$$= p(\gamma_j | \tilde{\gamma}_j), \quad (12c)$$

where (A) follows by assuming that $p(\gamma_j | \mathbf{r}_j) = p(\gamma_j)$, which means that the location is not informative about the RSS in the absence of further information. In other words, the medium is uniform and the set of possible environments ϵ is large enough not to favour any location over the others. This establishes the targeted approximation.

REFERENCES

- [1] K. B. Letaief, W. Chen, Y. Shi, J. Zhang, and Y.-J. Zhang, "The roadmap to 6G: AI empowered wireless networks," *IEEE Commun. Mag.*, vol. 57, no. 8, pp. 84–90, 2019.
- [2] D. Wu, Y. Zeng, S. Jin, and R. Zhang, "Environment-aware and training-free beam alignment for mmWave massive MIMO via channel knowledge map," in *IEEE Int. Conf. Comm. Workshops*, Jun. 2021, pp. 1–7.
- [3] Z. Xiao, T. He, P. Xia, and X.-G. Xia, "Hierarchical codebook design for beamforming training in millimeter-wave communication," *IEEE Trans. Wireless Commun.*, vol. 15, no. 5, pp. 3380–3392, 2016.
- [4] T. S. Cousik, V. K. Shah, J. H. Reed, T. Erpek, and Y. E. Sagduyu, "Fast initial access with deep learning for beam prediction in 5G mmWave networks," in *IEEE Mil. Commun. Conf.*, 2021, pp. 664–669.
- [5] K. Ma, D. He, H. Sun, and Z. Wang, "Deep learning assisted mmWave beam prediction with prior low-frequency information," in *IEEE Int. Conf. Comm.*, 2021, pp. 1–6.
- [6] Z. Wang, N. Chen, and M. Okada, "Deep learning-based variable scaling beam training for massive MIMO mmWave systems," in *IEEE Int. Symp. Comm. Inform. Tech.*, 2022, pp. 7–11.
- [7] M. Zecchin, M. B. Mashhadi, M. Jankowski, D. G., M. Kountouris, and D. Gesbert, "LIDAR and position-aided mmWave beam selection with non-local CNNs and curriculum training," *IEEE Trans. Veh. Technol.*, vol. 71, no. 3, pp. 2979–2990, 2022.
- [8] R. Maiberger, D. Ezri, and M. Erlihson, "Location based beamforming," in *IEEE 26-th Conv. Elect. Electro. Eng.*, 2010, pp. 000184–000187.
- [9] D. Romero and S.-J. Kim, "Radio map estimation: A data-driven approach to spectrum cartography," *IEEE Signal Process. Mag.*, vol. 39, no. 6, pp. 53–72, 2022.
- [10] Y. Zeng, J. Chen, J. Xu, D. Wu, X. Xu, S. Jin, X. Gao, D. Gesbert, S. Cui, and R. Zhang, "A tutorial on environment-aware communications via channel knowledge map for 6G," *IEEE Comm. Surveys & Tutorials*, 2024.
- [11] D. Romero, T. N. Ha, R. Shrestha, and M. Franceschetti, "Theoretical analysis of the radio map estimation problem," *arXiv preprint arXiv:2310.15106*, 2023.
- [12] H. B. Yilmaz, T. Tugcu, F. Alagöz, and S. Bayhan, "Radio environment map as enabler for practical cognitive radio networks," *IEEE Commun. Mag.*, vol. 51, no. 12, pp. 162–169, Dec. 2013.
- [13] R. Shrestha, T. N. Ha, P. Q. Viet, and D. Romero, "Radio map estimation: Empirical validation and analysis," *arXiv preprint arXiv:2310.11036*, 2024.
- [14] A. Alaya-Feki, S. B. Jemaa, B. Sayrac, P. Houze, and E. Moulines, "Informed spectrum usage in cognitive radio networks: Interference cartography," in *Proc. IEEE Int. Symp. Personal, Indoor Mobile Radio Commun.*, Cannes, France, Sep. 2008, pp. 1–5.
- [15] Y. Teganya and D. Romero, "Data-driven spectrum cartography via deep completion autoencoders," in *Proc. IEEE Int. Conf. Commun.*, Dublin, Ireland, Jul. 2020, pp. 1–7.
- [16] R. Shrestha, D. Romero, and S. P. Chepuri, "Spectrum surveying: Active radio map estimation with autonomous UAVs," *IEEE Trans. Wireless Commun.*, vol. 22, no. 1, pp. 627–641, 2022.
- [17] D. Romero, S.-J. Kim, G. B. Giannakis, and R. López-Valcarce, "Learning power spectrum maps from quantized power measurements," *IEEE Trans. Signal Process.*, vol. 65, no. 10, pp. 2547–2560, May 2017.
- [18] D. Romero, D. Lee, and G. B. Giannakis, "Blind radio tomography," *IEEE Trans. Signal Process.*, vol. 66, no. 8, pp. 2055–2069, Jan. 2018.
- [19] A. A. M. Saleh and R. Valenzuela, "A statistical model for indoor multipath propagation," *IEEE J. Sel. Areas Commun.*, vol. 5, no. 2, pp. 128–137, 1987.
- [20] C. M. Bishop, *Pattern Recognition and Machine Learning*, Information Science and Statistics. Springer, 2006.
- [21] S. M. Kay, *Fundamentals of Statistical Signal Processing, Vol. II: Detection Theory*, Prentice-Hall, 1998.